MICROMETEOROLOGICAL MEASUREMENT AND SOURCE REGION ANALYSIS OF NITROUS OXIDE FLUXES FROM AN AGRICULTURAL SOIL

F. G. WIENHOLD, M. WELLING and G. W. HARRIS*

Air Chemistry Department, Max Planck Institute for Chemistry, P.O. Box 3060, 55020 Mainz, Germany

Abstract—Nitrous oxide (N_2O) fluxes were measured by eddy correlation during a field experiment in August 1993. The measurements took place on a harvested wheat field located in northwest Sealand (Denmark). A tunable diode laser absorption spectrometer (TDLAS) was used for N_2O detection. The N_2O mixing ratio was sampled at a rate of 10 Hz synchronously with the three-dimensional wind data, air temperature, water vapour and carbon dioxide (CO_2) concentrations. Fast Fourier transform methods were applied to analyse spectral and co-spectral power distributions and to compute the fluxes from the covariance functions. Balance of the energy budget indicated adequate frequency coverage of the flux contributions. Continuous measurements were carried out in half hour intervals during daytime and fluxes in the range of 40–120 ng N m^{-2} s^{-1} were obtained. The footprint regions for the individual measurements were estimated by Markovian trajectory simulations taking into account the atmospheric stability conditions and wind distributions inferred from the micrometeorological measurements. The influence of adjoining fields with different crops was evident in the Bowen ratio and CO_2 flux, but not noticeable in the N_2O flux. This observation is consistent with supporting analysis of the soil depth dependence of the nitrous oxide production, which indicates that the major contributions arise from levels below 0.9 m.

Key word index: Flux measurements, eddy correlation, tunable diode laser spectroscopy, footprint analysis, Markovian trajectory simulation.

INTRODUCTION

The tropospheric nitrous oxide (N_2O) mixing ratio is increasing at a rate of 0.2–0.3% per year with a present average value of 310 ppbv (Intergovernmental Panel on Climate Change, IPCC, 1990). Transport through the tropopause and subsequent destruction in the stratosphere is the dominant atmospheric removal mechanism, leading to an atmospheric N_2O lifetime of approximately 130 yr (WMO, 1992). With this long lifetime, the observed N_2O rise corresponds to a 50% increase in the annual global source strength compared to the pre-industrial period, and a 40% excess of the present sources over the stratospheric sink (Prinn *et al.*, 1990). While the major N_2O sources probably have been identified, their individual contributions to the global budget remain highly uncertain (Houghton *et al.*, 1992). Emissions from cultivated soils are the most poorly understood, both in terms of their global source strength and the underlying microbial processes leading to N_2O production.

Recently, trace gas sensors providing sufficient accuracy and temporal resolution to quantify N_2O emissions by eddy correlation flux measurements have become available (Hargreaves *et al.*, 1994a; Wienhold *et al.*, 1994). In contrast to the commonly used chamber technique, the eddy correlation method derives the vertical turbulent flux density F_X of the target species X at the measurement point from the covariance between the vertical windspeed w and the trace gas concentration ρ_X: $F_X = \overline{w'\rho'_X}$. (Businger, 1986; Fowler and Duyzer, 1989). The primes indicate the deviations from the mean values (fluctuations), while the overbar denotes the time average. This results in a direct flux measurement in the sense that no further assumptions on turbulent atmospheric diffusion are required. The measurement point is located at a certain height inside the turbulent boundary layer downwind of the source region to be investigated, and therefore the measurement process itself does not interfere with the trace gas source, avoiding possible systematic errors. The method has the desired property of integrating the spatial variations of the emissions over a representative region, the size of which depends on the measurement height. However, atmospheric transport has to be stationary to ensure that the surface flux equals the flux detected at the measurement height, and a fetch (source region) with uniform morphology of the canopy is required. Such "ideal" circumstances are rarely met, especially with

respect to fetch uniformity, since although the topology of the region of interest may exhibit adequate flatness and lack aerodynamic obstacles, thereby allowing undisturbed turbulence, the actual field size (especially in Europe) is often too small to cover the entire measurement source region. In these circumstances, the analysis of the footprint areas for the individual measurements provides a valuable tool for data interpretation.

This paper describes measurements of N_2O emissions made by applying the eddy correlation method and the investigation of their spatial dependence using Markovian trajectory simulations. The experiment was part of a joint methods intercomparison field study carried out at Lammefjorden, Denmark, in August 1993, which combined chamber, eddy correlation and flux gradient techniques. A comparison of the results obtained by the different methods will be given elsewhere (Hargreaves *et al.*, 1994b).

EXPERIMENTAL SETUP

The measurement site was situated on a drained fjord in northwest Sealand (Denmark) which was reclaimed from the southern Kattegat in 1872. A flat region extends over several kilometers, with maximum elevations of less than 20 m. Steady, southwesterly sea-wind conditions were highly suitable for micrometeorological flux measurements. The soil has a high organic content and the groundwater table lay at ca. 1 m below the surface. Winter wheat had been harvested before the measurement campaign. Figure 1 shows the dimensions of the target and neighbouring fields as well as the location of the measurement devices. Although the field width was only ca. 100 m, the long side (more than 400 m) coincided with the prevailing wind direction. The arrangement for the micrometeorological measurements is shown in Fig. 2. The intake system (left half of the diagram) was set up at mast A indicated in Fig. 1, while the measurement van located 20 m downwind contained the spectrometer and the associated equipment. For eddy correlation measurements, air was sampled close to the measurement volume of a three-dimensional ultrasonic anemometer (Gill Instruments Ltd., Hampshire, U.K.) mounted at a height of 3.25 m above the

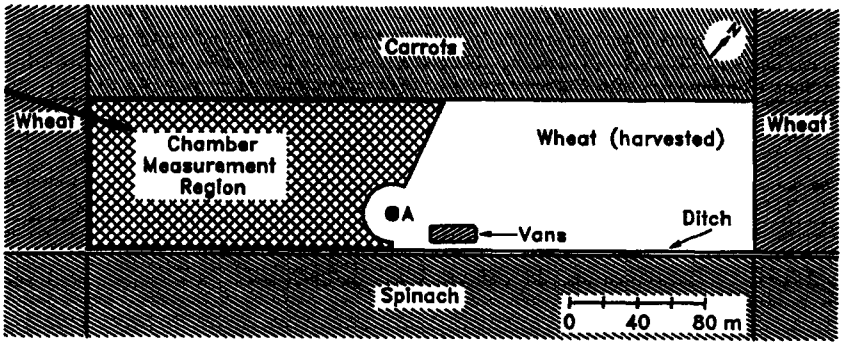

Fig. 1. Setup and environment of the field experiment. The mast ⊗A was used for the eddy correlation measurements. The large arrow indicates the prevailing wind direction.

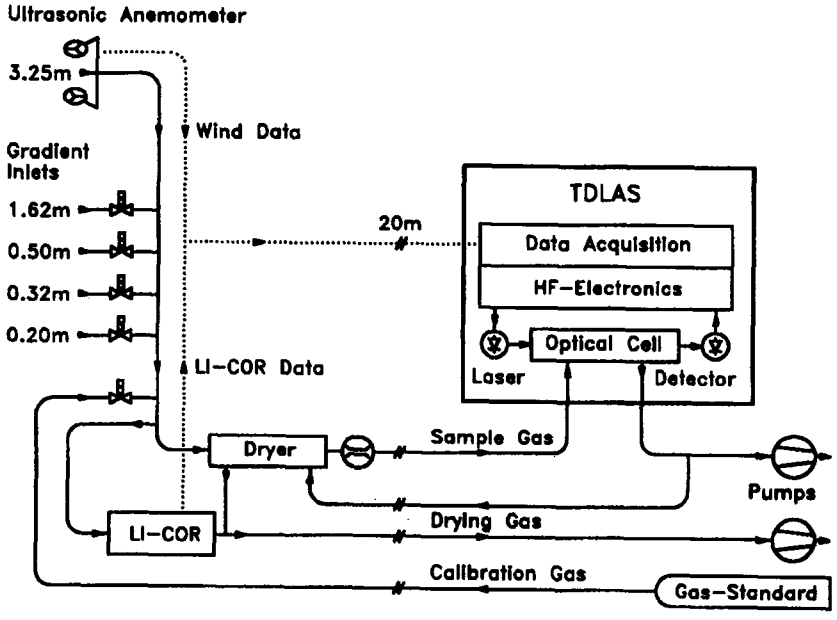

Fig. 2. Schematic diagram of the intake system (left half, situated at mast A in Fig. 1) and the spectrometer (right half, inside the measurement van).

ground. Additional inlets mounted on the mast could be used for gradient measurements which were carried out at selected times during the campaign for intercomparison purposes. A small fraction of the gas flow was branched to a non-dispersive infrared H_2O/ CO_2-analyser (LI-COR Inc., Nebraska, U.S.A., 10 Hz sampling frequency) for latent heat and CO_2 flux measurements. The water vapour content of the main gas flow was reduced by a factor of over 60 using a multitube dryer (two stages model PD–1000-24, Perma Pure Inc., Toms River, U.S.A.). Temperature equilibration of the sample gas was achieved by highly turbulent flow conditions in the intake line (Reynolds number $\geq$ 16,000) before entering the measurement cell of the tunable diode laser absorption spectrometer (TDLAS). This avoids the need to apply density corrections to the N_2O flux measurement (Webb *et al.*, 1980). However, they remained necessary for the supporting CO_2 measurement where the sample air could not be dried. These corrections and the associated errors are relevant when the trace gas fluxes are small with respect to the ambient concentration, i.e. for small transport velocities, which was the case for both CO_2 and N_2O fluxes. Damping of the N_2O concentration fluctuations in the intake section was characterized by a cut-off frequency of $\approx$7 Hz (Lenshow and Raupach, 1991) for the given flow conditions, which is high compared to the measurement cell gas exchange rate (see below). The CO_2 channel of the LI-COR instrument and the TDLAS were calibrated in half hour intervals using standard gases with ambient mixing ratios.

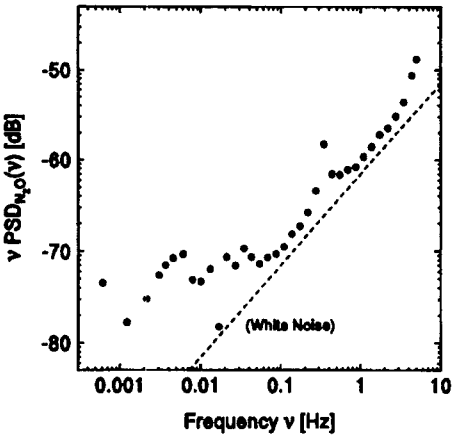

Fig. 3. Noise and drift of the TDLAS. The spectrum was obtained by Fourier transformation of a one hour 10 Hz time series recording still air.

The TDLAS for N_2O detection has been described by Wienhold *et al.* (1994). In brief, the absorption of single rotational–vibrational N_2O line at 4.527 μm was quantified by scanning it with the monochromatic emission of a lead-salt diode laser at a rate of 1 kHz. To increase sensitivity, the light path was folded inside a multi-reflection absorption cell (White, 1976; Roths, 1992) providing a total path of 46 m. The cell was purged by the sample gas with an exchange time of 200 ms. Experimental investigations confirmed that this gas exchange rate determined the overall N_2O measurement time response. The cell pressure was 40 mbar, which helps to avoid interferences arising from absorptions by other atmospheric constituents. High frequency modulation of the laser emission and phase sensitive detection (Cooper and Warren, 1987) were used to suppress laser, detector and electronic noise to a level which allowed sufficient precision in a signal averaging time of 0.1 s. Concurrent with the acquisition of a new spectrum, the N_2O mixing ratio and its error estimate were derived from the preceding spectrum by a linear least-square fit against a calibration spectrum. The noise and stability characteristics of the spectrometer were investigated by recording a continuous 1 h time series of measurements of N_2O in laboratory air at a sampling rate of 10 Hz. Figure 3 shows the power spectral density derived from this series by Fourier transformation; a level of 0 dB corresponds to the ambient mixing ratio (310 ppbv). Apart from a slight oscillation at 0.3 Hz, the characteristic is well represented by white noise over two orders of magnitude in frequency, before it becomes limited by spectrometer drift at a level below $-$ 70 dB, equivalent to a 100 pptv precision. This spectrometer performance was consistently reproduced under field conditions.

The TDLAS time response limits the bandwith of the data set. Therefore, the spectrometer was made to govern the

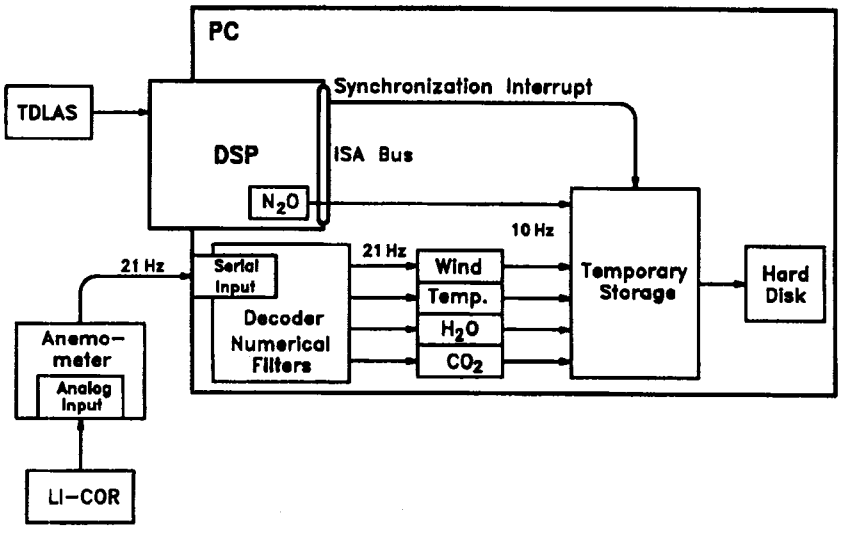

Fig. 4. Data acquisition timing. Wind, temperature, water vapour and CO_2 mixing ratio were read continuously by a personal computer (PC) and low pass filtered to match the N_2O measurement time response. The TDLAS data reduction algorithm carried out by a digital signal processor (DSP) triggered the synchronous sampling of the individual data streams.

overall eddy correlation data acquisition as shown in Fig. 4. Control of the spectrometer and analysis of spectra were carried out by a dedicated digital signal processor (DSP) connected to a AT-486 personal computer (PC) via the ISA-AT-bus. Synchronization between the two computers was established using a high-priority AT-interrupt to prevent timing problems otherwise caused by disk operation and other devices. Parallel to the operation of the spectrometer, the data stream from the sonic anemometer was continuously read through a PC serial port at a rate of 21 Hz. In addition to the three-dimensional wind vector, this data stream included information about air temperature (deduced from the sonic measurement), the readouts of the LI-COR analyser and control sequences. These data were processed by a decoding routine which checked data validity and passed the values to numerical low pass filters to reduce the higher bandwith to the bandwidth of the N_2O signal. Whenever a new N_2O mixing ratio was evaluated by the DSP (i.e. at a 10 Hz rate) the synchronization interrupt triggered the transfer of a complete data set to an array for temporary storage. At convenient time intervals, the array content was written to the hard disk. Continuous time series of 2^{14} data sets were acquired, resulting in 27.3 min measurement times between calibrations, and a frequency coverage of 6.1×10^{-4}–5 Hz according to the sampling theorem (Press *et al.*, 1988).

DATA ANALYSIS

The vertical fluxes of N_2O, CO_2, horizontal momentum, sensible and latent heat were determined off-line by evaluating the covariance of the corresponding time series with the vertical component w of the wind vector $\mathbf{u} = (u, v, w)$. Prior to the computation, the wind vectors were rotated to orientate the u-axis in the mean wind direction and to align the w-axis perpendicular to the average shear plane (McMillen, 1988). The resulting tilt angles for the vertical axis lay in a range of $\pm 3°$, indicating good pre-alignment of the anemometer and further indicating minimal flow distortion induced by the instrumental setup. The time series were Fourier transformed using a FFT algorithm, and the co-spectrum of two series was obtained by multiplying one transform with the conjugate complex of the other. Time shifts Δt_M introduced by the inlet tubes and the different instrument response times were accounted for by an appropriate phase angle rotation in the frequency domain, i.e. by multiplying the co-spectrum by $\exp(2\pi i \Delta t_M \nu)$, where ν denotes the channel frequency. In this way, the co-spectrum represented the power spectral density distribution. Mean values were suppressed by setting the channel corresponding to $\nu = 0$ equal to zero. In the presence of unwanted background in the covariance function, the co-spectrum was high pass filtered using cut-off frequencies in the range of $1–5 \times 10^{-3}$ Hz. Time and frequency were normalized and made dimensionless by using the scal-

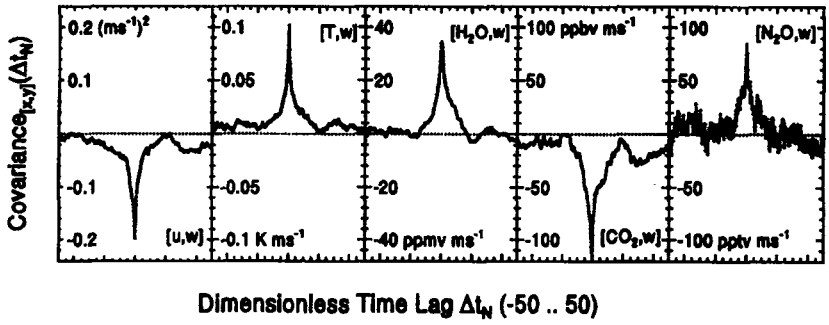

Fig. 5. Covariance functions for vertical fluxes of horizontal momentum, sensible heat, latent heat, CO_2 and N_2O. The flux magnitudes were calculated from the peaks at $\Delta t_N = 0$.

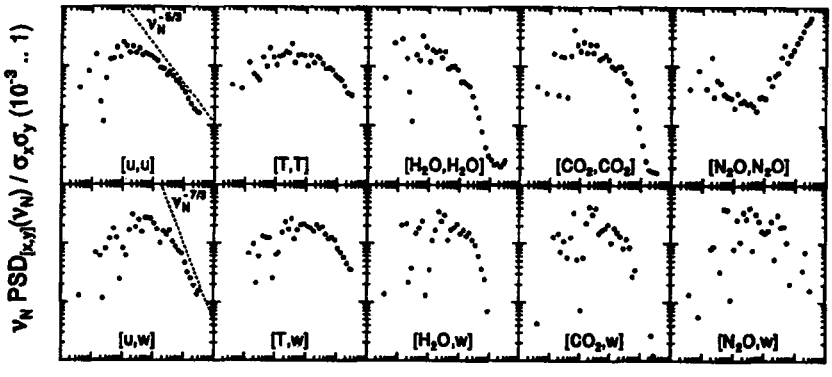

Fig. 6. Spectra and co-spectra corresponding to the data of Fig. 5.

ing factor $\bar{u}/h$ ($h = 3.25$ m being the measurement height), thus the normalized time and frequency are $\Delta t_N = \Delta t\,\bar{u}/h$ and $\nu_N = \nu(\bar{u}/h)^{-1}$.

Figure 5 illustrates a typical example of the resulting covariance functions in a time lag interval of $-50 \leqslant \Delta t_N \leqslant 50$, which contains the relevant information. The maxima and minima at $\Delta t_N = 0$ indicate upward or downward fluxes respectively: horizontal momentum and CO_2 are transferred towards the ground, whereas latent and sensible heat as well as N_2O are emitted. For the determination of the flux, a background value computed from the averages in the regions $-50 \leqslant \Delta t_N \leqslant -40$ and $40 \leqslant \Delta t_N \leqslant 50$ was subtracted from the peaks. The standard deviation of these intervals was used to estimate the error in the flux determination and the flux detection limit. For the N_2O flux measurements, an average detection limit of 6 pptv m s^{-1} (7.5 ng N m^{-2} s^{-1}) was obtained, while measured N_2O fluxes ranged from 40 to 120 ng N m^{-2} s^{-1}.

Figure 6 displays the power spectra and co-spectra corresponding to the data in Fig. 5. For the wind components and the sensible heat, the forms of these functions are in good agreement with results reported for the inertial subrange, e.g. by Kaimal *et al.* (1972). At the high frequency end, the finite time response of the LI-COR sensor becomes noticeable in the latent heat and CO_2 data. The TDLAS noise contribution is evident in the high frequency region of N_2O power spectrum, while at low frequencies the concentration fluctuations caused by the N_2O flux become obvious (compare Fig. 3). In the co-spectrum of N_2O and w however, the prominent high frequency signature of the spectrometer noise disappears completely, indicating the strong filtering capacity of the covariance function for uncorrelated fluctuations.

While the N_2O flux determination was of central interest, atmospheric stability conditions were also characterized by computing the friction velocity $u_* = \sqrt{\overline{u'w'}}$ and Monin-Obukhov-Length $L = -c_p\rho u_*^3\theta/kg(F_H + 0.07F_{LE})$ from the momentum and energy fluxes. Here, c_p, ρ and θ denote specific heat, air density and the potential temperature respectively. These parameters were used in the trajectory simulations described below.

SOURCE REGION MODELLING

Lagrangian trajectory simulations have widely been discussed and applied to the analysis of turbulent dispersion (Sawford, 1985). In contrast to most investigations aiming to elucidate general aspects of turbulent transport and their dependence on boundary conditions, we employed trajectory simulations in this study to examine source region effects on the actual trace gas emission measurements. This is highly desirable because of the conditions under which the experiment was conducted (see Fig. 1). We applied a model of limited complexity to estimate the source regions for the individual flux measurements using moderate computer resources and incorporating as far as possible the actual micrometeorological measurement results.

The model described by Leclerc and Thurtell (1990), based on the work of Wilson *et al.* (1981a–c), was adapted for our purpose. The trajectory of an air parcel originating at the ground was simulated by producing a series of positions for discrete time steps Δt,

$$\mathbf{x}_{n+1} = \mathbf{x}_n + \mathbf{u}_n\Delta t, \tag{1}$$

with $\mathbf{u}_n = (u_n, v_n, w_n)$ being the parcel velocity at the position $\mathbf{x}_n$. Whenever the trajectory crossed the plane of measurement it was taken as making a contribution to the flux measured at that height. Thus the horizontal source distribution of the air parcels contributing to the measured fluxes could be calculated.

For the vertical velocity of the air parcel a Markov chain

$$w_n = w_{n-1}e^{-\Delta t/\tau_L} + (1 - e^{-2\Delta t/\tau_L})^{1/2}\sigma_w r_n \tag{2}$$

was generated by low-pass filtering random numbers $\sigma_w r_n$ distributed with the measured vertical wind variance σ_w^2 and using the Lagrangian time scale $\tau_L = \int_0^\infty R_w(\tau)\,d\tau$ as the filter time constant. $R_w(\tau)$ denotes the vertical wind auto-correlation function. The horizontal displacement was derived from the vertical profile of the horizontal wind appropriate for the measured atmospheric stability (see below). As described by Wilson (1981c), the computations were performed in a coordinate system (x, y, z_*, t_*) with height independent scales $\tau_L = \tau_L(h)$, $\sigma_w = \sigma_w(h)$ and constant time steps $\Delta t_* = 0.1\,\tau_L(h)$, i.e. for homogeneous turbulence. Inhomogeneity of the turbulence was introduced by the coordinate transformation $(x, y, z_*, t_*) \rightarrow (x, y, z, t)$

$$\frac{dt_*}{\tau_L(h)} = \frac{dt}{\tau_L(z)}, \quad \frac{dz_*}{\Lambda(h)} = \frac{dz}{\Lambda(z)} \tag{3}$$

using the Lagrangian length scale

$$\Lambda = \sigma_w\tau_L. \tag{4}$$

This results in a transformation of the vertical wind component according to

$$\frac{w_*}{\sigma_w(h)} = \frac{w}{\sigma_w(z)}. \tag{5}$$

For a given data set, equations (3) were integrated using the empirical scales (Wilson *et al.*, 1981c)

$$\Lambda(z) = 0.5\,z\left(1 - 6\frac{z}{L}\right)^{1/4}, \quad L < 0 \tag{6}$$

$$\Lambda(z) = 0.5\,z\left(1 + 5\frac{z}{L}\right)^{-1}, \quad L \geqslant 0 \tag{7}$$

and (Leclerc and Thurtell, 1990)

$$\sigma_w(z) = 1.25u_* \left(1 + 4.1\frac{z}{L}\right)^{1/3}, \quad L < 0 \qquad (8)$$

$$\sigma_w(z) = \text{const.} = \sigma_w(h), \quad L \geqslant 0 \qquad (9)$$

for the cases of unstable ($L < 0$) and neutral to stable ($L \geqslant 0$) atmospheric conditions. These relations define the Lagrangian time scale τ_L via equation (4). Equation (8) was scaled by the vertical wind variance $\sigma_w(h)$ which was deduced directly from the measurements, thereby eliminating the empirical u_*-dependence. Numerical inversion of the integration results lead to the desired relations $t = t(t_*)$ and $z = z(z_*)$.

We endeavoured to use as many as possible of the measured micrometeorological data in the simulations, and therefore the random velocity values for the Markov chain [equation (2)] values were generated to match the measured w distribution instead of a Gaussian assumption. This was achieved by numerically inverting the integral of the measured frequency distribution and taking the values of the inverse function for white random arguments from the interval [0 ... 1] (transformation method). Similarly, the measured two-dimensional horizontal wind distribution was reproduced by random numbers to evaluate the horizontal wind profile as a function of the stability parameter z/L for each individual trajectory.

A 20 m × 20 m grid extended over a simulated source region of 1.6 km × 1.6 km with the inlet location in its centre, while the z_* axis was divided into 256 equidistant intervals, the measurement height corresponding to the 200th level. Typically 8000 trajectories were generated, starting from the ground and ending after leaving the top level. Flux contributions for the grid point corresponding to the distance travelled were counted positive or negative whenever the trajectory crossed the measurement level in upward or downward direction. The construction of the footprint pattern consumed 20–30 min of simulation time on an 33 MHz AT-486 computer.

Figure 7 shows a typical area source contribution simulated for a single flux measurement and the parent horizontal wind distribution for this footprint. The target wheat field is superimposed on the foot-

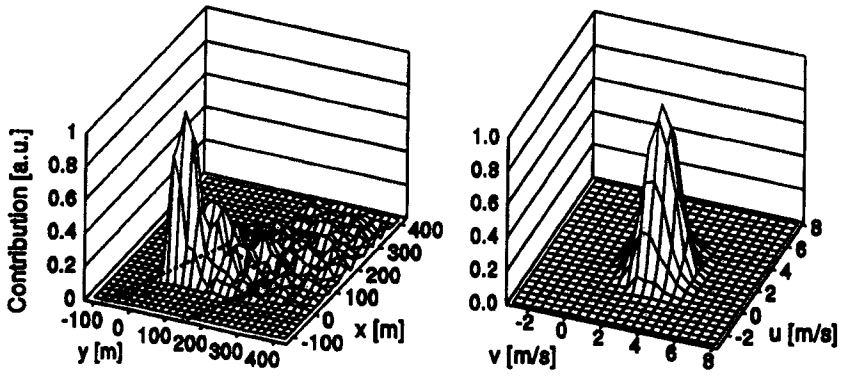

Fig. 7. Distributions of the relative source contribution (left) and the parent horizontal wind (right) for one individual flux measurement. The sampling point lies in the origin of the left-handed anemometer coordinate system. The limits of the wheat field are indicated by the dashed line. The footprint was integrated over this area to obtain the fractional wheat field contribution used in Figs 10 and 11.

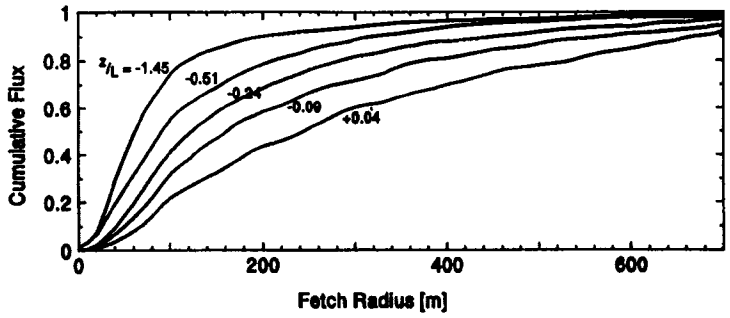

Fig. 8. Integrated radial footprint contribution parametrized by stability conditions as inferred during the campaign.

print pattern in the figure. The area covered by the flux measurements was found to be primarily dependent on atmospheric stability, as indicated in Fig. 8. The radial flux contribution was obtained from the two-dimensional footprint by angular integration. The results agree with the detailed study carried out by Leclerc and Thurtell (1990). The area sizes of the source regions were quantified for the individual measurements by calculating the minimum surface area contributing 50% of the total flux (Schmidt, 1994). For the predominant unstable to slightly stable conditions they ranged between 0.5 and 4×10^4 m^2.

RESULTS AND DISCUSSION

The systematic error that could arise from the limited bandwidth of the eddy correlation measurements was investigated by verifying closure of the energy balance for the sensible and latent heat fluxes (F_H and F_{LE}), net radiation (F_{NR}) and soil heat flux (F_S): $F_H + F_{LE} = F_{NR} + F_S$. While sensible and latent heat were measured by the eddy correlation system with the same bandwidth as the N_2O flux determination, the remaining net radiation and soil heat flux were recorded independently by a radiometer and soil heat flux plates (Hargreaves, private communication). Figure 9 demonstrates the generally good agreement of the results obtained by the different methods for the whole measurement period. Systematic errors in the eddy correlation measurements due to inadequate sampling speed, which would lead to an underestimation of the measured flux, are found to be of minor importance. Additional systematic errors, such as those arising from non-stationary transport conditions, can also be estimated from this analysis. Taking — as a worst case assumption for the eddy correlation measurements — the radiation and soil heat flux as "exact" values, the agreement of the energy flux estimates indicates the maximum error contribution to be of the order of 18%.

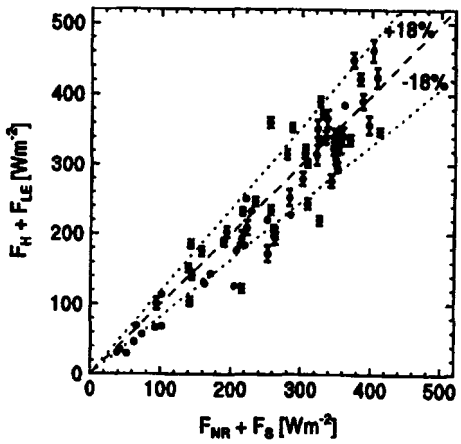

Fig. 9. Energy balance of the total atmospheric heat flux $F_H + F_{LE}$ and the sum of net radiation F_{NR} and soil heat flux F_S for the whole measurement period.

Flux data are presented in Fig. 10 for 27 August 1993. Although the diurnal cycle is obvious in the sensible and latent heat fluxes, it cannot be observed

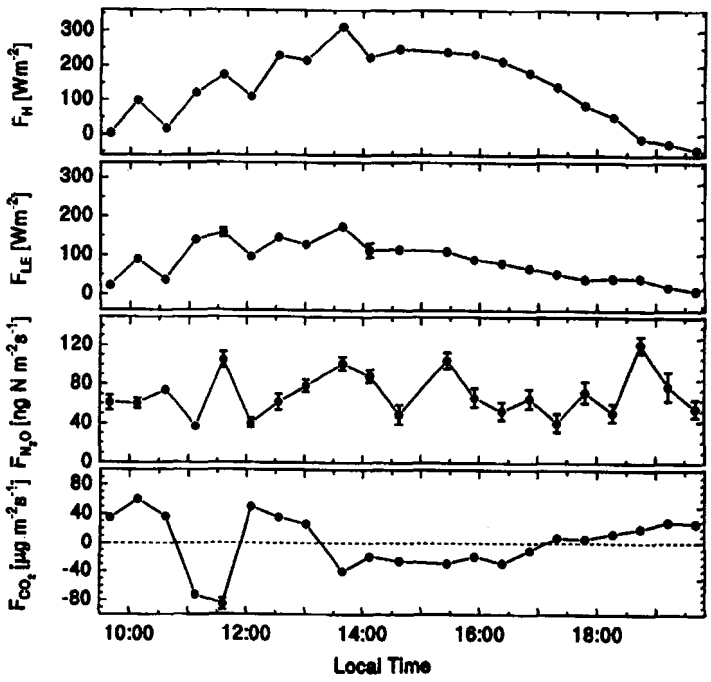

Fig. 10. Diurnal variation of the measured fluxes on 27 August 1993.

in the nitrous oxide flux. During the day, the CO_2 flux changes its direction several times without any correlation to the heat fluxes driven by solar irradiation. To clarify this situation, which is typical for the whole campaign period, we analysed influence of the source region on the measured fluxes. The fractional contribution of the harvested wheat field area (see Fig. 1) to each flux value measured by eddy correlation was evaluated by integrating the normalized fetch distribution calculated by the model over that area (see Fig. 7). The contributions were between 10% and 60%, depending on wind direction and atmospheric stability. Plant activity, which differentiated the adjoining fields from the harvested wheat field, lead to spatial variation in source and sink strength for water vapour and CO_2 through respiration and photosynthesis. Therefore, the CO_2 flux and the Bowen ratio $\beta = F_H/F_{LE}$ were investigated as a function of the wheat field contribution in the footprint, for a subset of the data with a net radiation of greater than 100 W m^{-2}. The result is shown in Fig. 11. A highly significant correlation to the fractional wheat field contribution is observed for both the CO_2 flux ($P_c < 3 \times 10^{-7}$, $N = 46$) and the Bowen ratio ($P_c < 2 \times 10^{-6}$). Both the CO_2 uptake and lowered Bowen ratio, i.e. enhanced water evaporation, are attributable to plant activity. The same analysis was carried out for the N_2O flux (Fig. 12). Here, a systematic dependence of the emissions on the source region is not observed, implying that the N_2O emissions from the soil were independent of the canopy when integrated over the footprint area of a few hectares. This finding simplifies the intercomparison of the results of different methods for estimating N_2O fluxes (chamber, eddy correlation, etc.) even for the case of an imperfect overlap of the source regions. From soil gas profiles that were taken during the campaign, the main production of N_2O (more than 90%) was found to occur at a depth of 0.9 m (Christensen, private communication). This is consistent with our micrometeorological observation of negligible canopy influence on the N_2O emissions.

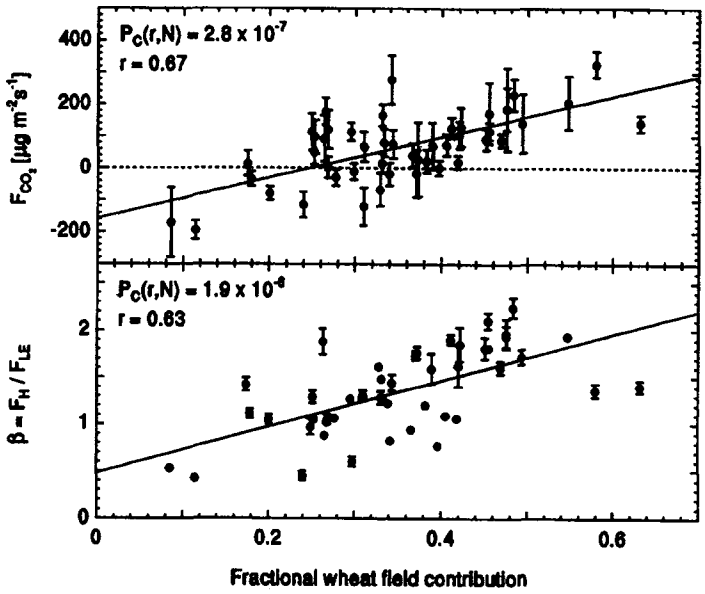

Fig. 11. Source region dependence of CO_2 uptake and Bowen ratio.

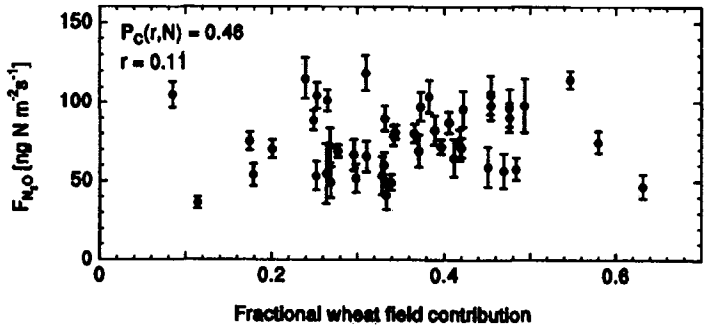

Fig. 12. Source region dependence of the N_2O emissions.

SUMMARY

We conducted eddy correlation flux measurements of N_2O emissions from an agricultural soil using a TDLAS as trace gas sensor. The N_2O flux detection limits were 7.5 ng N m^{-2} s^{-1} with measured fluxes ranging from 40 to 120 ng N m^{-2} s^{-1}. The vertical fluxes of momentum, sensible heat, latent heat and CO_2 were also measured by eddy correlation. Systematic errors estimated from closure of the energy balance were less than about 18%, and the errors resulting from the limited instrumental time response were found to be of minor importance. The supporting micrometeorological measurements were used to characterize the stability of the boundary layer. Lagrangian trajectory simulations were carried out for the individual measurements to analyse the footprint regions. A significant source region dependence was observed in the energy and CO_2 fluxes, but not in the N_2O fluxes. The footprint analysis was found to be very useful for data interpretation, and is sufficiently straightforward that it could be carried out in the future during the measurement period itself using computational resources available in the field.

REFERENCES

Businger J. A. (1986) Evaluation of the accuracy with which dry deposition can be measured with current micrometeorological techniques. *J. Clim. appl. Met.* **25**, 1100–1124.

Cooper D. E. and Warren R. E. (1987). Two-tone optical heterodyne spectroscopy with diode lasers: theory of line shapes and experimental results. *J. Opt. Soc. Am. B* **4**, 470–480.

Fowler D. and Duyzer J. H. (1989) Micrometeorological techniques for the measurement of trace gas exchange. In *Exchange of Trace Gases Between Terrestrial Ecosystems and the Atmosphere* (edited by Andreae M. O. and Schimel D. S.), pp. 189–207. Wiley, New York.

Hargreaves K. J., Fowler D., Skiba U., Milne R., Smith K. A. and Zahniser M. (1994a) Eddy covariance measurements of trace gas fluxes in northern Europe by tunable diode laser spectroscopy. European Geophysical Society XIX General Assembly, Grenoble, France, 25–29 April 1994. Abstract in *Ann. Geophys.* **12**, Supplement II, C 389.

Hargreaves K. J., Wienhold F. G., Klemedtsson L., Arah J. R. M., Beverland I., Fowler D., Galle B., Griffith D., Harris G. W., Skiba U., Smith K. A. and Welling M. (1994b) Measurement of nitrous oxide emissions from agricultural land using micrometeorological methods. *Atmospheric Environment* (submitted).

Houghton J. T., Callander B. A. and Varney S. K. (1992) *Climate Change 1992: The Supplementary Report to the IPCC Scientific Assessment*. Intergovernmental Panel on Climate Change, Cambridge University Press, Cambridge.

Intergovernmental Panel on Climate Change, IPCC (1990) *Climate Change, The IPCC Scientific Assessment*. Cambridge University Press, New York.

Kaimal J. C., Wyngaard J. C., Izumi Y. and Coté O. R. (1972) Spectral characteristics of surface-layer turbulence. *Q. J. R. Met. Soc.* **98**, 563–589.

Leclerc M. Y. and Thurtell G. W. (1990) Footprint prediction of scalar fluxes using a Markovian analysis. *Boundary-Layer Met.* **52**, 247–258.

Lenshow D. H. and Raupach M. R. (1991) The attenuation of fluctuations in scalar concentrations through sampling tubes. *J. geophys. Res.* **96**, 15,259–15,268.

McMillen R. T. (1988) An eddy correlation technique with extended applicability to non-simple terrain. *Boundary-Layer Met.* **43**, 213–245.

Press W. H., Flannery B. P., Teukolsky S. A. and Vetterling W. T. (1988) *Numerical Recipes in C*, pp. 398–404. Cambridge University Press, New York.

Prinn R., Cunnold D., Rasmussen R., Simmonds P., Alyea F., Crawford A., Fraser P. and Rosen R. (1990) Atmospheric emissions and trends of nitrous oxide deduced from 10 years of ALE–GAGE data. *J. geophys. Res.* **96** (*D*11), 18369–18385.

Roths J. (1992) Development of an airborne laser spectroscopic trace gas sensor and its deployment during the TROPOZ–II aircraft measurement campaign. Ph.D. thesis, pp. 67–70, Fachbereich Phys., Johannes-Gutenberg-Univ., Mainz, Germany (in German).

Sawford B. L. (1985) Lagrangian statistical simulation of concentration mean and fluctuation fields. *J. Clim. appl. Met.* **24**, 1152–1166.

Schmidt H. P. (1994) Source areas for scalars and scalar fluxes. *Boundary-Layer Met.* **67**, 293–318.

Webb E. K., Pearman G. I. and Leuning R. (1980) Correction of flux measurements for density effects due to heat and water vapor transfer. *Q. J. R. Met. Soc.* **106**, 85–100.

White J. U. (1976) Very long optical paths in air. *J. Opt. Soc. Am.* **66**, 411–416.

Wienhold F. G., Frahm H. and Harris G. W. (1994) Measurement of N_2O fluxes from fertilized grassland using a fast response tunable diode laser spectrometer. *J. geophys. Res.* **99** (*D*8), 16,557–16,567.

Wilson J. D., Thurtell G. W. and Kidd G. D. (1981a) Numerical simulation of particle trajectories in inhomogeneous turbulence, I: Systems with constant turbulent velocity scale. *Boundary-Layer Met.* **21**, 295–313.

Wilson J. D., Thurtell G. W. and Kidd G. D. (1981b) Numerical simulation of particle trajectories in inhomogeneous turbulence, II: Systems with variable turbulent velocity scale. *Boundary-Layer Met.* **21**, 432–441.

Wilson J. D., Thurtell G. W. and Kidd G. D. (1981c) Numerical simulation of particle trajectories in inhomogeneous turbulence, III: Comparison of predictions with experimental data for the atmospheric surface layer. *Boundary-Layer Met.* **21**, 443–463.

World Meteorological Organization, WMO (1992) Scientific assessment of ozone depletion: 1991, WMO/UNEP. World Meteorological Organization Global Ozone Research and Monitoring Project. Rep. 25, Geneva.